

# Channel Orthogonalization in Panel-Based LIS

Juan Vidal Alegría\*, Ove Edfors\*

\*Department of Electrical and Information Technology, Lund University, Lund, Sweden  
juan.vidal\_alegria@eit.lth.se, ove.edfors@eit.lth.se

**Abstract**—Large intelligent surface (LIS) has gained momentum as a potential 6G-enabling technology that expands the benefits of massive multiple-input multiple-output (MIMO). On the other hand, orthogonal space-division multiplexing (OSDM) may give a promising direction for efficient exploitation of the spatial resources, analogous as what is achieved with orthogonal frequency-division multiplexing (OFDM) in the frequency domain. To this end, we study how to enforce channels orthogonality in a panel-based LIS scenario. Our proposed method consists of having a subset of active LIS-panels coherently serving a set of users, and another subset of LIS-panels operating in semi-passive mode by implementing a receive and re-transmit (RRTx) process. This results in an inter-symbol interference (ISI) channel, where we characterize the semi-passive processing required to achieve simultaneous orthogonality in time and space. We then employ the remaining degrees of freedom (DoFs) from the orthogonality constraint to minimize the semi-passive processing power, where we derive a closed-form global minimizer, allowing for efficient implementation of the proposed scheme.

**Index Terms**—Large intelligent surface (LIS), Orthogonal space-division multiplexing (OSDM), Channel orthogonalization, Inter-symbol interference (ISI) channel.

## I. INTRODUCTION

Large intelligent surface (LIS) [1] is a technology which extends the concept of massive multiple-input multiple-output (MIMO) [2], [3] by considering whole walls covered with electromagnetic active material serving a set of user equipments (UEs) within the same time-frequency resource. The main potential of LIS mainly derives from its increased spatial resolution, allowing to multiplex users not only in the angular domain, but also in the depth domain [1], [4], thus leading to improved spectral efficiency beyond that of massive MIMO.

The main theoretical results on LIS—also found under the term holographic MIMO—have relied upon modeling it as a continuous surface of electromagnetically active material [1]. However, practical implementations of LIS may potentially consist of a discrete set of antennas deployed throughout large surfaces, which has firm equivalence with the continuous counterpart as proved in [1], [5]. Moreover, practical deployments may also favor panel-based LIS approaches, where a LIS is divided into several panels of antennas which may be distributed throughout large areas [6], [7].

As remarked in the literature [4], [8], [9], having distributed panels of antennas coherently serving a set of UEs leads to critical issues in terms of interconnection bandwidth and centralized processing complexity. These issues may be tackled by employing decentralized approaches where the panels may preprocess the received signals before combining them and/or sending them to a central processing unit (CPU) [10]–[13]. In this work, we propose an alternative approach to relieve these issues which consists of using only a subset of active LIS-panels for jointly decoding the data from the UEs, while the remaining panels operate in a *semi-passive* mode with the aim

of easing the decoding task of the active panels. Specifically, we consider employing the semi-passive panels to enforce channel orthogonality in space—as well as time—allowing for orthogonal space-division multiplexing (OSDM).

The idea of OSDM was considered in [14] as a counterpart to orthogonal frequency-division multiplexing (OFDM) for the spatial domain, which offers a convenient framework for efficient decoding and resource allocation in MIMO-based systems. Initial results from [14] show how to achieve orthogonal multi-user MIMO channels through the use of passive reconfigurable surfaces, where the freedom in the orthogonality constraint is employed to assure the passive nature of reconfigurable surfaces. In the current work, we however consider the use of LIS-panels for achieving channel orthogonality by implementing a receive and retransmit (RRTx) process using a subset of the LIS-panels in semi-passive mode. The main difference is that, in order to maintain coherence and synchronization using baseband processing at the LIS-panels, the signals retransmitted through the RRTx process are delayed one time-slot before arriving the active LIS-panels, thus generating an inter-symbol interference (ISI) channel. One important benefit of the current approach over those using passive surfaces [14], [15] is that the narrowband channel assumption is now accurate for OFDM-based systems since the baseband processing units allow to perform independent processing per subcarrier—unlike passive networks.

As happened in [14], [16], the orthogonality restriction still allows for some of degrees of freedom (DoFs), which may be hereby employed to minimize the power of the semi-passive processing—similar to what was done in [14], [16] when trying to fulfill the passive constraints. In the current framework, we have however been able to characterize in closed-form the global minimizers of the semi-passive processing power. This also gives an important advancement over [14], [16], where the solution to the analogous optimization problems employed costly minimization algorithms whose convergence to a global minimizer could not be formally assured.

The rest of the paper is organized as follows. Section II introduces the considered system model. In Section III, we show how to perform channel orthogonalization in the considered framework. In Section IV, we derive the closed-form solution to the power minimization problem. Section V includes a numerical evaluation of the proposed methods. Section VI concludes the paper with some final remarks.

## II. SYSTEM MODEL

Let us consider a panel-based LIS scenario<sup>1</sup> where a total of 3 LIS-panels are employed to decode the uplink transmission

<sup>1</sup>Equivalence with cell-free massive MIMO scenarios is evident by noting the correspondence between a LIS-panel and a distributed multi-antenna AP.

of  $K$  UEs through a narrow-band channel (e.g., one OFDM subcarrier). For simplicity, all LIS-panels are assumed to have the same number of antennas  $M \geq K$ , although extension of this work to LIS-panels with different combinations of antenna numbers is straightforward. On the other hand, we believe that the 3-panel scenario captures the essence of the proposed solution, but in the extended version we may formalize the results for an arbitrary number of LIS-panels.

Out of the 3 LIS-panels, only 1 panel is used for actively receiving and decoding the data from the UEs. The 2 remaining LIS-panels operate in *semi-passive* mode, where they jointly implement a receive and retransmit (RRTx) process. In this process one of the semi-passive LIS-panels—referred to as the semi-passive receive (SP-Rx) panel—is used for receiving the signals being exchanged between the UEs and the active panel, while the other one—referred to as the semi-passive transmit (SP-Tx) panel—is used for simultaneously transmitting the signals previously received at the respective SP-Rx panel. In the RRTx process, the semi-passive panels may also apply some linear processing which may be physically performed at the baseband processing unit of either (or both) of the panels. Effectively, the processing achieved by the semi-passive panels is analogous to that achieved by the fully-reconfigurable intelligent surface (FRIS) model with relaxed power constraints, defined in [14]. However, we now have the extra limitation that the reflected signals are delayed due to the RRTx process. The received vector at the active panel at time-slot  $t$ , is then given by

$$\mathbf{y}[t] = \mathbf{H}_0 \mathbf{s}[t] + \mathbf{H}_1 \Theta \mathbf{r}[t-1] + \mathbf{n}[t], \quad (1)$$

where  $\mathbf{H}_0$  is the  $M \times K$  channel matrix between the UEs and the active panel,  $\mathbf{H}_1$  is the  $M \times M$  channel between the SP-Tx panel and the active panel,  $\mathbf{r}[t]$  is the received vector at the SP-Rx panel at time-slot  $t$ ,  $\Theta$  is the equivalent linear-processing applied in throughout the RRTx process, and  $\mathbf{n}[t] \sim \mathcal{CN}(\mathbf{0}, N_0 \mathbf{I}_M)$  models the additive white Gaussian noise (AWGN) added at the active panel at time-slot  $t$ . We may express  $\mathbf{r}[t]$  recurrently by

$$\mathbf{r}[t] = \mathbf{H}_2 \mathbf{s}[t] + \mathbf{H}_{12} \mathbf{r}[t-1] + \tilde{\mathbf{n}}[t], \quad (2)$$

where  $\mathbf{H}_2$  is the  $M \times K$  channel between the UEs and the SP-Rx panel,  $\mathbf{H}_{12}$  is the  $M \times M$  channel between the SP-Tx and the SP-Rx panels, and  $\tilde{\mathbf{n}}[t] \sim \mathcal{CN}(\mathbf{0}, \tilde{N}_0 \mathbf{I}_M)$  models the AWGN added at the SP-Rx.

### III. ISI CHANNEL ORTHOGONALIZATION

We begin this section by considering two simplifying assumptions that will make the problem more tractable, while still matching to a great extend realistic scenarios. The validity of the first of these assumptions will be further reinforced by the results from Sections IV and V.

*Assumption 1:* If we consider the fact that the semi-passive processing may be optimized such that it does not require large amounts of amplification, we may assume that the noise term added in the RRTx process is negligible in (1). Note that this extra noise term appears multiplied by  $\Theta$  in (1) so it may have non-diagonal covariance—i.e., leading to colored noise—while a small norm for  $\Theta$  will also reduce the impact of the noise added by the RRTx process compared to the

white noise term  $\mathbf{n}[t]$ . Assuming negligible noise from the RRTx process thus means that the resulting noise will remain approximately white.

*Assumption 2:* Considering that the panels may be conveniently placed within scenario, we may assume that the semi-passive panels are located such that the channel between them is negligible. For example, we could have one facing the main user locations, and the other one facing the active panel. We may thus take the assumption  $\mathbf{H}_{12} \approx \mathbf{0}$  such that we can get rid of the recurrence associated to (2).<sup>2</sup>

Considering Assumptions 1 and 2, we may rewrite (1) as

$$\mathbf{y}[t] = \mathbf{H}_0 \mathbf{s}[t] + \tilde{\mathbf{H}}(\Theta) \mathbf{s}[t-1] + \mathbf{n}[t], \quad (3)$$

where the  $M \times K$  matrix  $\tilde{\mathbf{H}}(\Theta) = \mathbf{H}_1 \Theta \mathbf{H}_2$  corresponds to the aggregate channel associated to the RRTx process. Note that, assuming full-rank  $\mathbf{H}_1$  and  $\mathbf{H}_2$ , as well as unrestricted semi-passive processing  $\Theta$ , we have full freedom in designing  $\tilde{\mathbf{H}}(\Theta)$ . For example, this could be achieved by canceling  $\mathbf{H}_2$  in the SP-Rx panel—multiplying the left pseudo-inverse—and then cancelling  $\mathbf{H}_1$  in the SP-Tx panel—multiplying the inverse—after applying the desired processing on the signal coming from the SP-Rx panel. We may also note that, if Assumption 1 does not apply, the noise term in (3) would be colored, hence compromising the optimality of symbol-by-symbol detection from the orthogonal channels—it would correspond to a pseudo-zero forcing solution instead. However, the results that we show next would still lead to channel orthogonality in the desired signal part of (3).

As can be seen from (3), due to the RRTx process, the received vector suffers from ISI, thus compromising the orthogonality property in the time domain. Considering  $T$  consecutive symbol transmissions within the coherence time, and assuming  $\mathbf{s}[t] = \mathbf{0}$  for  $t = 0$  and  $t = T + 1$ , we may write the complete received vector as

$$\mathbf{y}_C = \mathcal{H} \mathbf{s}_C + \mathbf{n}_C, \quad (4)$$

where  $\mathbf{y}_C$  is a  $(T+1)M \times 1$  vector stacking up the received vectors  $\mathbf{y}[t]$  at  $t = 1, \dots, T+1$ ,<sup>3</sup>  $\mathbf{s}_C$  is a  $TK \times 1$  vector stacking up the transmitted symbol vectors  $\mathbf{s}[t]$  at  $t = 1, \dots, T$ ,  $\mathbf{n}_C$  is the corresponding  $(T+1)M \times 1$  AWGN vector, and  $\mathcal{H}$  is the resulting  $(T+1)M \times TK$  ISI channel matrix, which considers simultaneously the space and the time domain. From (3), we may express  $\mathcal{H}$  as

$$\mathcal{H} = \begin{bmatrix} \mathbf{H}_0 & \mathbf{0} & \dots & \mathbf{0} \\ \tilde{\mathbf{H}}(\Theta) & \mathbf{H}_0 & \ddots & \vdots \\ \mathbf{0} & \tilde{\mathbf{H}}(\Theta) & \ddots & \mathbf{0} \\ \vdots & \ddots & \ddots & \mathbf{H}_0 \\ \mathbf{0} & \dots & \mathbf{0} & \tilde{\mathbf{H}}(\Theta) \end{bmatrix}. \quad (5)$$

In order to achieve simultaneous orthogonality in time and space, the ISI channel should fulfill

$$\mathcal{H}^H \mathcal{H} = \beta \mathbf{I}_{TK}. \quad (6)$$

<sup>2</sup>Note that, even if  $\mathbf{H}_{12}$  is not exactly  $\mathbf{0}$ , every step in the recursion would attenuate its contribution due to the repeated path-loss being experienced.

<sup>3</sup>We assume that the receiver may be active for one more time-slot than the transmission duration so that it can listen to the last retransmission. For large  $T$ , this would have negligible effect on the overall performance.

Note that we may also relax (6) by allowing the right-hand side (RHS) to be an arbitrary diagonal matrix instead of a scaled identity. However, this would lead to having different channel capacity for different UEs, or under different time-slots, which is generally not as desirable as enforcing a fair rate distribution by considering (6) (see [14]). Nevertheless, many of our results may be trivially extended to that case. Considering (5), we may operate the left-hand side (LHS) of (6) to reach

$$\mathcal{H}^H \mathcal{H} = \begin{bmatrix} \mathbf{G}(\Theta) & \mathbf{Z}^H(\Theta) & \mathbf{0} & \dots & \mathbf{0} \\ \mathbf{Z}(\Theta) & \mathbf{G}(\Theta) & \mathbf{Z}^H(\Theta) & \ddots & \vdots \\ \mathbf{0} & \mathbf{Z}(\Theta) & \mathbf{G}(\Theta) & \ddots & \mathbf{0} \\ \vdots & \ddots & \ddots & \ddots & \mathbf{Z}^H(\Theta) \\ \mathbf{0} & \dots & \mathbf{0} & \mathbf{Z}(\Theta) & \mathbf{G}(\Theta) \end{bmatrix}, \quad (7)$$

where we have defined the  $K \times K$  matrices

$$\mathbf{G}(\Theta) = \mathbf{H}_0^H \mathbf{H}_0 + \widetilde{\mathbf{H}}^H(\Theta) \widetilde{\mathbf{H}}(\Theta) \quad (8a)$$

$$\mathbf{Z}(\Theta) = \mathbf{H}_0^H \widetilde{\mathbf{H}}(\Theta). \quad (8b)$$

The orthogonality constraint, given in (6), can then be translated into the following conditions

$$\mathbf{G}(\Theta) = \beta \mathbf{I}_K \quad (9a)$$

$$\mathbf{Z}(\Theta) = \mathbf{0}_{K \times K}. \quad (9b)$$

Taking into account the expression for  $\mathbf{Z}(\Theta)$  in (8b), in order to fulfill (9b)  $\Theta$  should be selected such that the columns of  $\widetilde{\mathbf{H}}(\Theta)$  fall in the null-space of  $\mathbf{H}_0^H$ . Since we have unrestricted  $\Theta$ ,  $\widetilde{\mathbf{H}}(\Theta)$  may be arbitrarily selected to fulfill said restriction. Let us express the singular value decomposition (SVD) of  $\mathbf{H}_0$  as

$$\mathbf{H}_0 = \mathbf{U}_0 \begin{bmatrix} \Lambda_0^{\frac{1}{2}} \\ \mathbf{0} \end{bmatrix} \mathbf{V}_0, \quad (10)$$

where  $\mathbf{U}_0$  and  $\mathbf{V}_0$  are the respective  $M \times M$  and  $K \times K$  unitary matrices, and  $\Lambda_0^{\frac{1}{2}}$  is the  $K \times K$  diagonal matrix with the singular values along the diagonal. We may then select

$$\widetilde{\mathbf{H}}(\mathbf{B}) \triangleq \widetilde{\mathbf{H}}(\Theta_s(\mathbf{B})) = \mathbf{U}_0 \begin{bmatrix} \mathbf{0}_{K \times K} \\ \mathbf{B} \end{bmatrix}, \quad (11)$$

where  $\mathbf{B}$  corresponds to an  $(M-K) \times K$  matrix which may be arbitrarily selected. Note that (11) generalizes any  $M \times K$  matrix falling in the null-space of  $\mathbf{H}_0^H$ . Moreover,  $\Theta_s(\mathbf{B})$  may be trivially obtained from (11) by inverting  $\mathbf{H}_1$  and  $\mathbf{H}_2$  as

$$\Theta_s(\mathbf{B}) = \mathbf{H}_1^{-1} \widetilde{\mathbf{H}}(\mathbf{B}) \mathbf{H}_2^\dagger, \quad (12)$$

where  $\mathbf{H}_2^\dagger$  corresponds to the left pseudo-inverse of  $\mathbf{H}_2$ —which may have multiple solutions. Alternative solutions may consider the inversion of the cascaded channel ( $\mathbf{H}_2^\dagger \otimes \mathbf{H}_1$ ) associated to the vectorized version of (12).<sup>4</sup>

Selecting  $\widetilde{\mathbf{H}}(\Theta)$  by (11) allows to fulfill the restriction (9b), while maintaining the remaining DoF in the selection of  $\mathbf{B}$ .

<sup>4</sup>The reader may refer to [14] for detailed results on the connection between  $\Theta$  and  $\widetilde{\mathbf{H}}(\Theta)$  under architectures leading to various restrictions on  $\Theta$ .

Next, we would like to determine  $\mathbf{B}$  such that (9a) can be simultaneously fulfilled, leading to channel orthogonalization. Considering (11) and (8a), equation (9a) leads to

$$\mathbf{B}^H \mathbf{B} = \beta \mathbf{I}_K - \mathbf{H}_0^H \mathbf{H}_0. \quad (13)$$

The previous equation is only solvable whenever we can match the rank of the two sides. For an generic  $\mathbf{H}_0$ —i.e., excluding those in a set of measure 0—and assuming  $M \geq K$ , the right-hand side is of full-rank  $K$  with probability 1. Thus, we also need the LHS to be of full-rank  $K$ , which leads to the orthogonalization condition

$$M \geq 2K, \quad (14)$$

where we considered that  $\text{rank}(\mathbf{B}^H \mathbf{B}) \leq \min(M-K, K)$ . Assuming (14) is fulfilled, (13) can be solved by selecting

$$\mathbf{B}(\widetilde{\mathbf{U}}) = \widetilde{\mathbf{U}}(\beta \mathbf{I}_K - \Lambda_0)^{\frac{1}{2}} \mathbf{V}_0^H, \quad (15)$$

where  $\widetilde{\mathbf{U}}$  is a semi-unitary matrix of dimension  $(M-K) \times K$ , i.e.,  $\widetilde{\mathbf{U}}^H \widetilde{\mathbf{U}} = \mathbf{I}_K$ , which may be arbitrarily selected. The result in (15) corresponds to the selection  $\mathbf{B} = (\beta \mathbf{I}_K - \mathbf{H}_0^H \mathbf{H}_0)^{\frac{1}{2}}$ , but we have expressed it in terms of its SVD to outline the DoFs left after enforcing the orthogonality constraint, which are captured in the selection of  $\widetilde{\mathbf{U}}$ . In fact, these DoFs can be used to reduce the power requirements for performing the RRTx process, as will be discussed in the next section. On the other hand, the selection (15) also leads to an extra orthogonalization condition given by

$$\beta \geq \lambda_{0,\max}, \quad (16)$$

where  $\lambda_{0,\max}$  corresponds to the greatest eigenvalue of  $\mathbf{H}_0^H \mathbf{H}_0$ —i.e., the greatest diagonal element of  $\Lambda_0$ . This comes from avoiding square roots of negative diagonal elements in (15), which would not allow to fulfill (13) since the resulting matrix should be positive semi-definite. The condition (16) may be understood as the minimum channel gain required to be able to compensate the direct channel, which may be matched to a minimum power requirement for the semi-passive panels.

#### IV. POWER MINIMIZATION

In Section III, we have shown how to achieve perfect orthogonalization of the ISI channel resulting from using two isolated LIS-panels for relaying an uplink transmission to an active LIS-panel. Condition (14) delimits the possibility to perform channel orthogonalization in this framework, so let us assume this condition is fulfilled—which is reasonable in typical LIS scenarios where  $M \gg K$ . Let us also assume that  $\beta$  is fixed such that (16) is fulfilled, which may be achieved by adjusting the amplification in the RRTx process. As previously mentioned, the orthogonalization restriction still allows for DoFs which may be suitably exploited to enforce desirable properties on the processing applied throughout the RRTx process. We will next study how to make use of these DoFs.

A major goal of the proposed scheme is to increase the overall energy efficiency by employing LIS-panels in a semi-passive (low-power) operation mode. Hence, we propose to use the DoFs available from the channel orthogonalization to

minimize the power of the processing applied at the semi-passive panels. Said power may be measured in terms of the squared Frobenius norm of the RRTx processing, leading to the following optimization problem

$$\begin{aligned} \min_{\tilde{\mathbf{U}}} \|\Theta_s(\tilde{\mathbf{U}})\|_{\text{F}}^2 \\ \text{s.t. } \tilde{\mathbf{U}}^{\text{H}}\tilde{\mathbf{U}} = \mathbf{I}_K, \end{aligned} \quad (17)$$

where we have  $\Theta_s(\tilde{\mathbf{U}}) \triangleq \Theta_s(\mathbf{B}(\tilde{\mathbf{U}}))$ , i.e., the RRTx processing is obtained from (12), using (11) and (15). Note that (17) is also relevant for increasing the validity of Assumption 1, since  $\|\Theta_s(\tilde{\mathbf{U}})\|_{\text{F}}^2$  multiplies the power of the noise associated to the RRTx process reaching (1). We may simplify the objective function in (17) by

$$\|\Theta_s(\tilde{\mathbf{U}})\|_{\text{F}}^2 \triangleq \text{tr}(\Theta_s^{\text{H}}(\tilde{\mathbf{U}})\Theta_s(\tilde{\mathbf{U}})) = \text{tr}(\check{\mathbf{H}}_1\tilde{\mathbf{U}}\check{\mathbf{H}}_2\check{\mathbf{H}}_2^{\text{H}}\tilde{\mathbf{U}}^{\text{H}}\check{\mathbf{H}}_1^{\text{H}}), \quad (18)$$

where we have defined

$$\check{\mathbf{H}}_1 \triangleq \mathbf{H}_1^{-1}\mathbf{U}_0 \begin{bmatrix} \mathbf{0}_{K \times (M-K)} \\ \mathbf{I}_{M-K} \end{bmatrix} \quad (19a)$$

$$\check{\mathbf{H}}_2 \triangleq (\beta\mathbf{I}_K - \Lambda_0)^{\frac{1}{2}}\mathbf{V}_0^{\text{H}}\mathbf{H}_2^{\dagger}. \quad (19b)$$

Since we want to solve (17), we may select without loss  $\mathbf{H}_2^{\dagger}$  as the Moore-Penrose inverse [17], since any other selection corresponds to adding a matrix in the left null-space of  $\mathbf{H}_2$ , which would give a positive additive term in  $\|\Theta_s(\tilde{\mathbf{U}})\|_{\text{F}}^2$ , i.e., leading to a suboptimal result.

The minimization problem defined in (17) is non-convex due to the semi-unitary constraint on  $\tilde{\mathbf{U}}$ . However, this constraint corresponds to restricting the search space to the Stiefel manifold  $\mathcal{S}(M-K, K)$ , which, when equipped with a Riemannian metric, gives a Riemannian manifold. We may then employ the Riemannian structure to solve (17) within the Stiefel manifold defined from its restrictions. Specifically, we will consider the results from [18], which studies the Riemannian structure of the unitary group under the bi-invariant Riemannian metric induced by the inner product  $\langle \mathbf{U}, \mathbf{V} \rangle = \frac{1}{2}\text{tr}(\mathbf{U}\mathbf{V}^{\text{H}})$ . Note that the particularization of results from the unitary group  $\mathcal{U}(M-K)$  to the Stiefel manifold  $\mathcal{S}(M-K, K)$  can be done by considering that any  $\tilde{\mathbf{U}} \in \mathcal{S}(M-K, K)$  corresponds to a projection of a unitary matrix  $\mathbf{U} \in \mathcal{U}(M-K)$  given by  $\tilde{\mathbf{U}} = \mathbf{U} \begin{bmatrix} \mathbf{I}_K & \mathbf{0} \end{bmatrix}^{\text{T}}$ .

Considering the Riemannian structure studied in [18] for the unitary group, we may express the Riemannian gradient at an arbitrary point  $\mathbf{U} \in \mathcal{U}(M-K)$  as

$$\tilde{\nabla} \mathcal{J}(\mathbf{U}) = \Gamma_{\mathcal{J}}(\mathbf{U}) - \mathbf{U}\Gamma_{\mathcal{J}}^{\text{H}}(\mathbf{U})\mathbf{U}, \quad (20)$$

where  $\Gamma_{\mathcal{J}}(\mathbf{U}) \triangleq \frac{\partial \mathcal{J}(\mathbf{U})}{\partial \mathbf{U}^*}$  corresponds to the Euclidean gradient of the objective function  $\mathcal{J}(\mathbf{U})$ .<sup>5</sup> Since we are interested in solving (17), the objective function corresponds to  $\mathcal{J}(\mathbf{U}) = \|\Theta_s(\mathbf{U} \begin{bmatrix} \mathbf{I}_K & \mathbf{0} \end{bmatrix}^{\text{T}})\|_{\text{F}}^2$ . We may note that, since the objective function  $\mathcal{J}(\mathbf{U})$  does not depend on the last  $(M-2K)$

<sup>5</sup>We consider differentiating only over the frame  $\partial \mathbf{U}^*$ , which does not span by itself the whole complex tangent space. However, since our analysis depends upon finding stationary points, while a stationary point under said frame equivalently corresponds to a stationary point under the frame  $\partial \mathbf{U}$  [19] (and vice-versa), we have no loss in differentiating only over  $\mathbf{U}^*$ .

columns of  $\mathbf{U}$ , the respective entries in  $\Gamma_{\mathcal{J}}(\mathbf{U})$  are 0. Through basic optimization arguments [20], the solution to (17) should be given either by a stationary point or by a boundary point. When particularizing the gradient to the underlying Riemannian structure, all the points now correspond to interior points, so the solution to (17) should be exclusively given by stationary points, i.e., such that the Riemannian gradient in (20) vanishes. The stationary points may then be found by solving the equation  $\tilde{\nabla} \mathcal{J}(\mathbf{U}) = 0$ . We then note that the  $(M-2K)$  columns of  $\mathbf{U}$  not appearing in  $\tilde{\mathbf{U}}$  have no impact on the stationary points of (20) since an equivalent equation to the previous one is obtained by multiplying by  $\mathbf{U}^{\text{H}}$  both sides from the right, so that in the resulting equation the respective columns of  $\mathbf{U}$  appear multiplied by the 0 entries in  $\Gamma_{\mathcal{J}}(\mathbf{U})$ . We thus reach the equivalent equation

$$\Gamma_{\mathcal{J}}(\tilde{\mathbf{U}})\tilde{\mathbf{U}}^{\text{H}} = \tilde{\mathbf{U}}\Gamma_{\mathcal{J}}^{\text{H}}(\tilde{\mathbf{U}}), \quad (21)$$

where the Euclidean gradient  $\Gamma_{\mathcal{J}}(\tilde{\mathbf{U}}) \triangleq \frac{\partial \mathcal{J}(\tilde{\mathbf{U}})}{\partial \tilde{\mathbf{U}}^*}$  corresponds to the non-zero part of  $\Gamma_{\mathcal{J}}(\mathbf{U})$ . From (18), we may get [21]

$$\Gamma_{\mathcal{J}}(\tilde{\mathbf{U}}) = \check{\mathbf{G}}_1\tilde{\mathbf{U}}\check{\mathbf{G}}_2, \quad (22)$$

where we have defined  $\check{\mathbf{G}}_1 = \check{\mathbf{H}}_1^{\text{H}}\check{\mathbf{H}}_1$  and  $\check{\mathbf{G}}_2 = \check{\mathbf{H}}_2\check{\mathbf{H}}_2^{\text{H}}$ . Substituting in (21) gives the following matrix equation

$$\check{\mathbf{G}}_1\tilde{\mathbf{U}}\check{\mathbf{G}}_2\tilde{\mathbf{U}}^{\text{H}} = \tilde{\mathbf{U}}\check{\mathbf{G}}_2^{\text{H}}\tilde{\mathbf{U}}^{\text{H}}\check{\mathbf{G}}_1^{\text{H}}. \quad (23)$$

The following lemma characterizes the unique set of solutions to (23) for any full-rank  $\check{\mathbf{G}}_1$  and  $\check{\mathbf{G}}_2$  with distinct eigenvalues. Note that this condition is fulfilled with probability 1 for generic  $\mathbf{H}_1$  and  $\mathbf{H}_2$  matrices. However, whenever it is not fulfilled, the solution to (17) described next may be extended by analogously exploiting the extra DoFs.

*Lemma 1:* Consider two arbitrary positive-definite matrices  $\check{\mathbf{G}}_1$  and  $\check{\mathbf{G}}_2$ , each of them containing distinct eigenvalues, and where we may assume without loss that the dimension of  $\check{\mathbf{G}}_1$  is larger than that of  $\check{\mathbf{G}}_2$ . The solutions to (23) with semi-unitary constraint on  $\tilde{\mathbf{U}}$  fulfill

$$\tilde{\mathbf{U}} = \check{\mathbf{U}}_1\mathbf{P}_1 \begin{bmatrix} \Lambda_{\varphi} \\ \mathbf{0} \end{bmatrix} \mathbf{P}_2\check{\mathbf{U}}_2^{\text{H}}, \quad (24)$$

where  $\check{\mathbf{U}}_1$  and  $\check{\mathbf{U}}_2$  are the unitary matrices from the eigenvalue decomposition (with decreasing eigenvalues) of  $\check{\mathbf{G}}_1$  and  $\check{\mathbf{G}}_2$ , respectively,  $\mathbf{P}$  is an arbitrary permutation matrix, and  $\Lambda_{\varphi}$  is a diagonal matrix with unit modulus entries along the diagonal.

*Sketch of Proof:* The proof consists of expressing  $\check{\mathbf{G}}_1$  and  $\check{\mathbf{G}}_2$  through their eigenvalue decompositions, and absorbing in  $\tilde{\mathbf{U}}$  their respective unitary matrices of eigenvectors by having  $\tilde{\mathbf{U}} = \check{\mathbf{U}}_1\tilde{\mathbf{U}}_2^{\text{H}}$ . The resulting equation is then solved by any  $\tilde{\mathbf{U}}$  that simultaneously diagonalizes  $\check{\mathbf{L}}_1$  and  $\check{\mathbf{L}}_2$ , corresponding to the respective diagonal eigenvalue matrices of  $\check{\mathbf{G}}_1$  and  $\check{\mathbf{G}}_2$ . Assuming  $\check{\mathbf{G}}_1$  has greater dimension than  $\check{\mathbf{G}}_2$ , and both matrices have distinct eigenvalues, the solutions are then trivially captured by (24). A complete proof may be included in the extended version.  $\square$

From Lemma 1, we may substitute (24) into (18), which leads to

$$\|\Theta_s\|_F^2 = \sum_{i=1}^K \check{\lambda}_{1,\pi_1(i)} \check{\lambda}_{2,\pi_2(i)}, \quad (25)$$

where  $\check{\lambda}_{1,i}$  and  $\check{\lambda}_{2,i}$  correspond to the  $i$ th eigenvalue of  $\check{\mathbf{G}}_1$  and  $\check{\mathbf{G}}_2$ , respectively, while  $\pi_1$  and  $\pi_2$  correspond to the  $(M-K)$ - and  $K$ -element permutations of associated to  $\mathbf{P}_1$  and  $\mathbf{P}_2$ , respectively. From (25), we can note that the diagonal values of  $\Lambda_\varphi$  have no impact whatsoever on the objective function since the corresponding phases cancel each other after being multiplied by their conjugates. We may thus select  $\Lambda_\varphi = \mathbf{I}_K$  without loss of generality. On the other hand, since only  $K$  of the  $M-K$  eigenvalues of  $\check{\mathbf{G}}_1$  appear in (25), we can trivially select  $\pi_1$ —through the respective  $\mathbf{P}_1$ —such that eigenvalues of  $\check{\mathbf{G}}_1$  appearing in (25) are the  $K$  eigenvalues with lower value. Alternatively, we may equivalently substitute  $\check{\mathbf{U}}_1$  in (24), associated to the eigenvalue decomposition of  $\check{\mathbf{G}}_1$  for increasing eigenvalues, with the respective unitary matrix associated to the eigenvalue decomposition for decreasing eigenvalues and select  $\mathbf{P}_1 = \mathbf{I}_{M-K}$ . In any case, we may trivially fix  $\mathbf{P}_1$  without loss, and the remaining DoFs are captured exclusively by  $\pi_2$  (or correspondingly  $\mathbf{P}_2$ ). Hence, with the previous considerations, the search space for the global minimum of (17) is reduced to evaluating the  $K!$  possible options for  $\pi_2$  in (25), and choosing the one attaining lowest value. However, we may further obtain a closed form optimal selection of  $\pi_2$  by considering the following lemma.

*Lemma 2:* Considering a finite increasing sequence  $\{\check{\lambda}_{1,i}\}_{1 \leq i \leq K}$  and an arbitrary permutation  $\pi_2$  of another finite increasing sequence  $\{\check{\lambda}_{2,i}\}_{1 \leq i \leq K}$ , the solution to

$$\min_{\pi_2} \sum_{i=1}^K \check{\lambda}_{1,i} \check{\lambda}_{2,\pi_2(i)} \quad (26)$$

is given by the permutation  $\pi_2^{\text{opt}}$  attaining a decreasing sequence  $\{\check{\lambda}_{2,\pi_2^{\text{opt}}(i)}\}_{1 \leq i \leq K}$ .

*Sketch of Proof:* The proof can be extended from the  $K=2$  case, where we can express  $\check{\lambda}_{1,1} = \check{\lambda}_{1,2} + \epsilon_1$  and  $\check{\lambda}_{2,1} = \check{\lambda}_{2,2} + \epsilon_2$  for some  $\epsilon_1, \epsilon_2 > 0$ . If we select  $\pi_2$  such that  $\{\check{\lambda}_{2,\pi_2(i)}\}_{1 \leq i \leq 2}$  is increasing instead of decreasing we get an extra additive term  $\epsilon_1 \epsilon_2$ , which is positive from the definition of  $\epsilon_1$  and  $\epsilon_2$ . Hence, the optimal choice is to have  $\pi_2$  such that  $\{\check{\lambda}_{2,\pi_2^{\text{opt}}(i)}\}_{1 \leq i \leq 2}$  is decreasing. A formal proof may be included in the extended version.  $\square$

If we put together Lemmas 1 and 2, as well as our observation on how to fix  $\mathbf{P}_1$ , we can obtain the closed form global optimum  $\check{\mathbf{U}}^{\text{opt}}$  to the minimization problem from (17)—up to some extra DoFs with no impact on  $\|\Theta_s(\check{\mathbf{U}})\|_F^2$ .

## V. NUMERICAL RESULTS

Due to the channel power requirement for the orthogonalization condition in (16), the power of the direct channel  $\mathbf{H}_0$ , which is linearly related to the maximum eigenvalue of  $\mathbf{H}_0^H \mathbf{H}_0$ , is one of the limiting factors to be able to efficiently implement the proposed scheme. Specifically, it is the relation between this channel and the gain of the channels  $\mathbf{H}_1$  and

$\mathbf{H}_2$  that matters, since these also scale the power of the retransmitted signals consequently processed to compensate the direct channel. Thus, we model  $\mathbf{H}_0$ ,  $\mathbf{H}_1$ , and  $\mathbf{H}_2$  as normalized IID Rayleigh fading channels [22], where the power of  $\mathbf{H}_0$  is scaled by a variable  $\eta$  giving the relation between the direct channel and the RRTx channel.<sup>6</sup>

In Fig. 1 (left), we show the average minimum semi-passive processing power required to achieve channel orthogonalization for different values of  $M$  and  $K$ . We include results for the optimized DoF selection from Section IV, as well as for a random selection, i.e., where  $\check{\mathbf{U}}$  in (15) is isotropically selected, which outlines the importance of our optimization method that allow to reduce the required power by roughly 10 dB. On the other hand, we include as comparison the optimization results from [16], which solves an equivalent optimization problem through geodesic gradient descent for two reflective surfaces, namely amplitude-reconfigurable intelligent surface (ARIS) and FRIS. For equal antenna combinations, the new results outperform those of ARIS, and, for weak direct channels, they also outperform FRIS. However, for greater direct channel gains, FRIS still requires lower processing power, which makes sense since applying per-subcarrier baseband processing makes our solution more robust, but it comes at the extra cost of having to compensate an ISI channel. Moreover, as outlined in [14], the complication of practical implementations of FRIS makes it mostly suitable as a theoretical construction that upper limits the capabilities of such systems, while our solution still performs close to it. On the other hand, we should not disregard the corresponding channel gain associated to these processing power curves, shown in Fig. 1 (right). We may note that the proposed method attains the same minimum  $\beta$  as that of FRIS, ARIS for the same antenna configurations, hinting that a similar rule to (16) may apply to such systems, while this was not formally proved yet in [14], [16].

Fig. 2 shows the sum capacity of the proposed method with and without considering Assumption 1. We have assumed that the power of the noise added at the semi-passive panels is the same as that of the noise added at the active panel, i.e.,  $\tilde{N}_0 = N_0$ . However,  $\tilde{N}_0$  could be actually lower when operating the semi-passive panels at low amplification, so that Assumption 1 may have better accuracy in reality than what is seen from Fig. 2. In any case, we see that this assumption is still accurate as long as the direct channel gain is not much greater than the gain of channels experienced by the RRTx process, while in general scenarios we may expect them to be in the same order. We have plotted for comparison the capacity achieved when the three panels are actively serving the UEs, giving a performance upper bound, as well as when the active LIS-panel serves the UEs by itself, giving a performance lower bound. However, we should note that our method has the extra advantage of achieving a perfectly orthogonal channel, which is not fulfilled by the other two cases. As expected, having 3 active LIS-panels has an important advantage when the direct channel gain is low, but comes at the cost of

<sup>6</sup>We are aware that the IID Rayleigh channel model may not be accurate when considering panel-based LIS scenarios since it disregards the inherent spatial correlation of panels [5], as well as the presence of strong line-of-sight paths [1]. However, it still allows us to assess the main limitations of our methods, which are mainly related to the rank and power of the considered channels, while it detaches them from specific geometries/implementations.

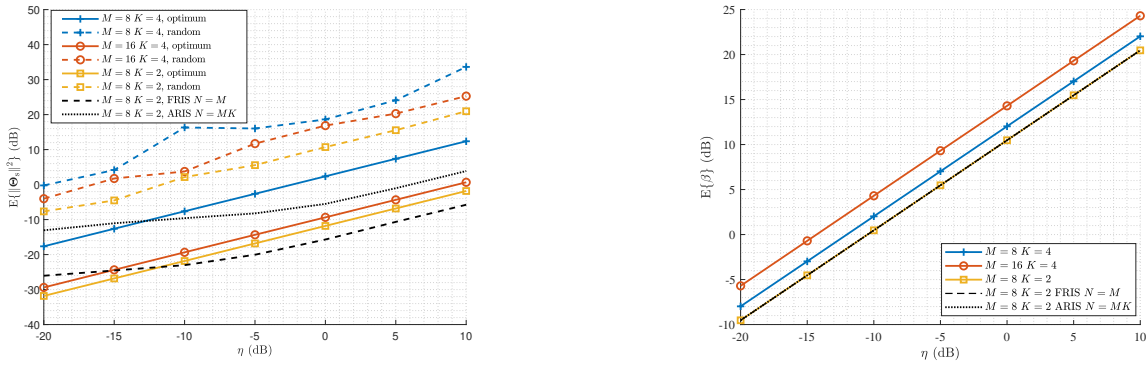


Fig. 1: Semi-passive power (left) for minimum channel gain per UE (right) with respect to the direct channel gain.

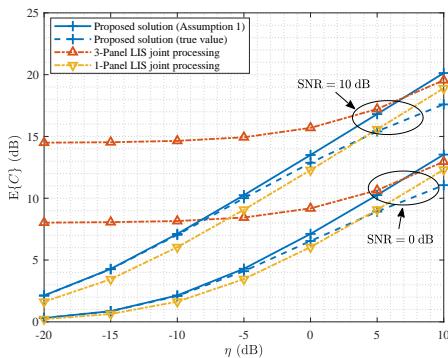


Fig. 2: Ergodic sum capacity with respect to direct channel gain for  $M = 8$  antennas per panel and  $K = 2$  UEs.

higher interconnection bandwidth, while our method still gets reasonably close performance as gain increases.

## VI. CONCLUSIONS

We have studied channel orthogonalization in a panel-based LIS scenario with a single active LIS-panel and two semi-passive LIS panels jointly implementing an RRTx scheme. We have derived the semi-passive processing required to perfectly orthogonalize the resulting channel, and characterized the conditions under which this is possible. We have also derived closed-form results on how to utilize the DoFs available from the orthogonality constraint to obtain (globally) minimum semi-passive processing power. The numerical results showcase the potential of the methods studied in this work.

## REFERENCES

- [1] S. Hu, F. Rusek, and O. Edfors, "Beyond massive MIMO: The potential of data transmission with large intelligent surfaces," *IEEE Transactions on Signal Processing*, vol. 66, no. 10, pp. 2746–2758, May 2018.
- [2] T. L. Marzetta, "Noncooperative cellular wireless with unlimited numbers of base station antennas," *IEEE Transactions on Wireless Communications*, vol. 9, no. 11, pp. 3590–3600, November 2010.
- [3] F. Rusek, D. Persson, B. K. Lau, E. G. Larsson, T. L. Marzetta, O. Edfors, and F. Tufvesson, "Scaling up MIMO: Opportunities and challenges with very large arrays," *IEEE Signal Processing Magazine*, vol. 30, no. 1, pp. 40–60, Jan 2013.
- [4] E. Björnson, L. Sanguinetti, H. Wymeersch, J. Hoydis, and T. L. Marzetta, "Massive MIMO is a reality—what is next?: Five promising research directions for antenna arrays," *Digital Signal Processing*, vol. 94, pp. 3–20, 2019, special Issue on Source Localization in Massive MIMO. [Online]. Available: <https://www.sciencedirect.com/science/article/pii/S1051200419300776>
- [5] A. Pizzo, T. L. Marzetta, and L. Sanguinetti, "Spatially-stationary model for holographic mimo small-scale fading," *IEEE Journal on Selected Areas in Communications*, vol. 38, no. 9, pp. 1964–1979, 2020.
- [6] A. Pereira, F. Rusek, M. Gomes, and R. Dinis, "Deployment strategies for large intelligent surfaces," *IEEE Access*, vol. 10, pp. 61 753–61 768, 2022.
- [7] M. Jung, W. Saad, Y. Jang, G. Kong, and S. Choi, "Performance analysis of large intelligent surfaces (LISs): Asymptotic data rate and channel hardening effects," *IEEE Transactions on Wireless Communications*, vol. 19, no. 3, pp. 2052–2065, 2020.
- [8] G. Interdonato, E. Björnson, H. Quoc Ngo, P. Frenger, and E. G. Larsson, "Ubiquitous cell-free massive mimo communications," *EURASIP Journal on Wireless Communications and Networking*, vol. 2019, no. 1, pp. 1–13, 2019.
- [9] S. Elhoushy, M. Ibrahim, and W. Hamouda, "Cell-free massive mimo: A survey," *IEEE Communications Surveys & Tutorials*, vol. 24, no. 1, pp. 492–523, 2022.
- [10] E. Björnson and L. Sanguinetti, "Scalable cell-free massive mimo systems," *IEEE Transactions on Communications*, vol. 68, no. 7, pp. 4247–4261, 2020.
- [11] J. Rodríguez Sánchez, F. Rusek, O. Edfors, and L. Liu, "Distributed and scalable uplink processing for lis: Algorithm, architecture, and design trade-offs," *IEEE Transactions on Signal Processing*, vol. 70, pp. 2639–2653, 2022.
- [12] J. Vidal Alegría, F. Rusek, and O. Edfors, "Trade-offs in decentralized multi-antenna architectures: The WAX decomposition," *IEEE Transactions on Signal Processing*, vol. 69, pp. 3627–3641, 2021.
- [13] F. Wiffen, W. H. Chin, and A. Doufexi, "Distributed dimension reduction for distributed massive MIMO c-ran with finite fronthaul capacity," in *2021 55th Asilomar Conference on Signals, Systems, and Computers*, 2021, pp. 1228–1236.
- [14] J. Vidal Alegría, J. Thunberg, and O. Edfors, "Channel orthogonalization with reconfigurable surfaces: General models, theoretical limits, and effective configuration," 2024.
- [15] T. Jiang and W. Yu, "Interference nulling using reconfigurable intelligent surface," *IEEE Journal on Selected Areas in Communications*, vol. 40, no. 5, pp. 1392–1406, 2022.
- [16] J. Vidal Alegría and F. Rusek, "Channel orthogonalization with reconfigurable surfaces," in *2022 IEEE Globecom Workshops (GC Wkshps)*, 2022, pp. 37–42.
- [17] R. A. Horn and C. R. Johnson, *Matrix Analysis*. Cambridge University Press, 1985.
- [18] T. E. Abruđan, J. Eriksson, and V. Koivunen, "Steepest descent algorithms for optimization under unitary matrix constraint," *IEEE Transactions on Signal Processing*, vol. 56, no. 3, pp. 1134–1147, 2008.
- [19] D. H. Brandwood, "A complex gradient operator and its application in adaptive array theory," in *IEE Proceedings H (Microwaves, Optics and Antennas)*, vol. 130, no. 1. IET Digital Library, 1983, pp. 11–16.
- [20] S. P. Boyd and L. Vandenberghe, *Convex optimization*. Cambridge university press, 2004.
- [21] A. Hjørungnes and D. Gesbert, "Complex-valued matrix differentiation: Techniques and key results," *IEEE Transactions on Signal Processing*, vol. 55, no. 6, pp. 2740–2746, 2007.
- [22] A. Paulraj, R. Nabar, and D. Gore, *Introduction to Space-Time Wireless Communications*, 1st ed. USA: Cambridge University Press, 2008.